Effect of Ag−Cu Alloy Nanoparticle Composition on Luminescence Enhancement/Quenching

Sanchari Chowdhury,[†] Venkat R. Bhethanabotla,*[,†] and Rajan Sen[‡]

Sensors Research Laboratory, Department of Chemical and Biomedical Engineering, and Department of Civil and Environmental Engineering, University of South Florida, Tampa, Florida 33620-5350

Received: January 12, 2009; Revised Manuscript Received: June 18, 2009

Metal enhanced/quenched luminescence was explored in the vicinity of Ag_xCu_{100-x} alloy nanoparticles at different compositions ($x = 100$, 67, 50, 30, and 0). These Ag−Cu nanoparticles were synthesized using the polyol process. It was observed that the luminescence of dyes was strongly dependent on the Ag−Cu nanoparticle composition. Highest luminescence enhancement of dye Cy 3, commonly used for biological applications, was achieved in the vicinity of pure silver nanoparticles. Enhancement effects were found to decrease as the percentage of copper was increased in the nanoparticles, leading to the quenching of fluorescence near pure copper nanoparticles. Theoretical calculations based on the corrected Gersten and Nitzan model[1] were carried out to predict the possible enhancement factors for spherical Ag−Cu nanoparticles for a range of compositions. Results of these calculations corroborate the experimental findings. Signal manipulation of luminescent dyes using the composition of alloy nanoparticles will extend applications of metal-enhanced luminescence to several fields ranging from optoelectronics to biological research.

I. Introduction

The emission of luminophores is significantly influenced in close proximity of conducting metallic nanostructures. Using nanoparticle platforms, it is possible to increase the quantum yield of weakly luminescent probes. This increase results from a modification of the radiative decay rate by coupling the emission with surface plasmon resonance (SPR) and by coupling emission at far field with nanoparticle scattering. These nanostructures can also enhance the excitation intensity experienced by vicinal luminophore molecules by enhancing the incident optical field by increasing the local field at the molecular location.[2−5] The presence of nanoparticles close to the luminophores can create new nonradiative channels due to light absorption inside the metal, thus quenching the emission of luminophores.[6] If the probe molecules are very close to the nanoparticles (typically, less than 5 nm), luminescence emission is quenched due to Förster transfer of energy from the excited state of the molecule to the surface plasmons of the metal surface. This quenching effect decreases with the cube of separation distance.[7] If the probes are too far from the nanoparticles, the influence of the nanoparticles is diminished. Hence, there exists an optimum separation distance for maximum emission enhancement/quenching.[8−12]

Metal-enhanced luminescence (MEL) has been studied mostly using silver nanoparticles[3−5,13−17] due to their intense and narrow SPR peaks. Gold nanoparticles are known to both quench and enhance luminescence depending on the fluorophore−particle separation distance, molecular dipole orientation with respect to particle surface, and size of the nanoparticles.[18−20] Relatively smaller (typically less than 30 nm) gold nanoparticles quench fluorescence emission due to nonradiative transfer from the excited states of luminophore molecules to the gold nanoparticles.[19] Larger gold nanoparticles can enhance luminescence due to the increased contribution of nanoparticle scattering.[18,21] Other metals such as copper and aluminum have been reported to enhance luminescence.[22,23] Recently, zinc oxide (ZnO) nanorod platforms have been reported to enhance luminescence intensity significantly from commonly utilized fluorophores in immunoassays.[24−26] Both enhancement and quenching of luminescence due to the proximity of nanoparticles are efficiently utilized for many different applications. Enhanced signal and photostability of luminophores, improved surface immunoassay and DNA detection, enhanced wavelength-ratiometric sensing, and amplified assay detection are few examples of the applications of MEL. On the other hand, quenching resulting from metallic nanoparticles has been successfully utilized for the improvement of homogeneous and competitive fluorescence immunoassay,[27,28] optical detection of DNA hybridization,[29] competitive hybridization assay,[30] and optoelectronics.[31]

There are some theoretical models explaining the influence of metal nanostructures on luminescence of dyes in the literature. Models based on exact electrodynamical theory[1,32] and the Gersten-Nitzan (GN) model[1,33,34] provide insight into the influence of metal nanospheres on radiative and nonradiative decay rates of luminophore molecules at close proximity. These theories explain that electromagnetic interaction between luminophore and metal nanostructures results in the increase of both radiative and nonradiative decay rates depending on luminophore−nanoparticle separation distance and the properties of the nanoparticles (size, shape, and dielectric constant), which decide the scattering and surface plasmon resonance behavior of the nanospheres. On the basis of these theories, it can be concluded that both radiative and nonradiative decay rates can be manipulated to result in luminescence enhancement or quenching by designing nanostructured platforms of particular shape, size, and composition. Mertens et al.[1,34] have corrected the G-N model to account for radiation damping and dynamic depolarization and have shown that results obtained using this corrected G-N model compare well with a model based on exact electrodynamics. This corrected G-N model is suitable for a

* Corresponding author. E-mail: venkat@eng.usf.edu.
[†] Department of Chemical and Biomedical Engineering.
[‡] Department of Civil and Environmental Engineering.

10.1021/jp900294z CCC: $40.75
Published on Web 07/06/2009

larger particle-size range than the original version. Kümmerlen et al.[16] presented a model that is based on the G-N model and includes both excitation enhancement by local field effects and the change in emission intensity due to radiative and nonradiative decay rate enhancement. In our study, we utilize a theoretical model based on theory proposed by Kümmerlen et al.[16] and Mertens et al.[1] to study the effect of composition of alloy nanoparticles on quantum efficiency enhancement.

SPR wavelength and scattering efficiency, the most important properties of nanostructures which dictate the enhancement/quenching of luminophore molecules,[14,35] can be manipulated by controlling any of the parameters of particle size, aspect ratio, shape, particle-to-particle distance, and surrounding dielectric medium.[14,36,37] Alloy nanoparticles offer additional degrees of freedom for tuning their optical properties by altering atomic composition and atomic arrangement,[38] thus can be an attractive option for manipulating the luminophore signal. Herein, we report the use of alloy nanoparticles for MEL. We demonstrate that by tuning the composition of alloy nanoparticles, the signal of vicinal luminophore can be manipulated. Due to their interesting optical properties, we chose silver−copper alloy nanoparticles as a material for our study.[39−42] The imaginary component of the dielectric constant of copper is significantly larger (more than twice) than that of silver in the wavelength range of 300 to 600 nm. Hence, it is expected that in this wavelength range, due to higher ohmic losses, Cu nanoparticles will mostly quench the luminescence at close proximity.[23] Further, the SPR spectrum of Ag is more intense and narrower than that of Cu nanoparticles. The absorption peak attributed to SPR occurs at shorter wavelengths for Ag. Hence, by modifying the composition and atomic arrangement we can tune both breadth and location of the peak of the SPR spectrum of Ag−Cu alloy nanoparticles.[39] We observed the effects of Ag−Cu alloy nanoparticles on the fluorescence emission from Cy3, a commonly used luminophore in biological applications. We chose Cy3 due to its low quantum yield (<0.04).[43] We found that the composition of alloy nanoparticles has a strong effect on MEL. We establish simple and straightforward routes for manipulating the brightness of emission from luminophore by changing the composition of the alloy nanoparticles.

II. Experimental Section

In this study, Ag−Cu nanoparticles of five different compositions were synthesized using the polyol process as described in ref 44. Silver nitrate (>99%), copper(II) acetate hydrate (98%), and polyvinylpyrrolidone (PVP, 55 000 molecular weight) were obtained from Sigma-Aldrich Co., MO, and used as received. The same volume of solution of PVP (1.0634 g in 20 mL ethylene glycol) was first added to ethylene glycol solution of copper salt (0.016 mols) and was then deaerated by bubbling with nitrogen for 30 min. The solution was then held at 175 °C for 20 min under nitrogen atmosphere, and a certain amount of $AgNO_3$−ethylene glycol solution was added to it. The reaction was then allowed to continue for another 5 min before bringing the system down to room temperature. Alloy nanoparticles of different compositions were synthesized by varying the molar ratio of silver and copper salts in the reaction mixture. With an increase in copper percentage, the color of the colloidal solution changed from yellowish to more reddish. Copper nanoparticles were synthesized following the same procedure except that the silver nitrate solution was replaced by the reducing agent ascorbic acid.

Glass substrates were silanized to immobilize silver−copper nanoparticles on them.[45] Glass slides were first cleaned with piranha solution for 30 min (1:3 30% hydrogen peroxide/concentrated sulfuric acid) (CAUTION! *Piranha solution reacts violently with most organic materials and should be handled with extreme care*). The cleaned glass substrates were silanized by immersing them in 2% 3-(aminopropyl)triethoxysilane (APS) solution in methanol for 2 h.[45] After this, the slides were rigorously cleaned with methanol followed by water to remove any excess APS. Ag−Cu nanoparticles were deposited on the APS coated glass slides by soaking them in freshly prepared solutions for specific times. Copper nanoparticles were immobilized on the glass slides following the procedure given by Male et al.[46] Piranha-cleaned glass slides were immersed in 20% poly(diallyldimethylammonium chloride)(PDDA, MW 200 000−350 000, Aldrich) aqueous solution for 16 h. Then, these slides were thoroughly rinsed with deionized water and dried in a nitrogen stream. These polymer-coated glass slides were incubated in Cu nanoparticle solution for 3 h. Finally, Cu nanoparticle coated glass slides were rinsed with deionized water and dried with nitrogen.

Silver nanoparticles were synthesized using the well-known Tollens reaction.[11] In summary, 10% ammonium hydroxide was added to 10 mL of aqueous $AgNO_3$ (0.1 M) while stirring. Once the initially formed brown precipitates dissolved, a 0.8 mol solution of NaOH in water was added to the solution. Preparation of Tollens reagent was completed by adding NH_4OH dropwise to the solution until the brown precipitate dissolved. The Tollens reagent was stored in a refrigerator for 30 min to reduce its temperature to ∼4 °C. For deposition of silver nanoparticles on glass substrates, equal amounts of the Tollens reagent and 0.5 M dextrose solution were mixed together and immediately drop-cast on a piranha-cleaned glass substrate followed by rinsing with deionized water after 1 min. The surface morphology of the nanostructures was observed and characterized by transmission electron microscopy (FEI Morgagni 268D), atomic force microscopy (Digital Instruments, Nanoscope IIIa), and scanning electron microscopy (Hitachi S-800). A UV−vis spectrometer (JASCO, V-530) was used for measuring the light extinction spectra attributed to the SPR of these nanoparticles. TEM samples were prepared by dispersing a few drops of Ag−Cu alloy nanoparticle solution on a carbon film supported by molybdenum grids.

Luminophore coatings on the nanoparticles and glass substrates were accomplished by dispersing Cy3-labeled streptavidin in 0.25% poly(vinyl alcohol) (PVA, MW 15 000) aqueous solution by sonicating and then coating the solution on the substrates by spin-coating (1500 rpm speed). The resulting polymer thickness was approximately 26 nm. Hence, the average distance between the substrate and a luminophore molecule was approximated by 13 nm. As the luminophores were coated following the same procedure for all samples, the separation distance between luminophore molecules and nanoparticles and the coverage of the luminophore molecules on nanoparticles are assumed to be the same for all samples.

A Leica DMI 4000b inverted fluorescence microscope equipped with a Leica DFC340 FX CCD camera was utilized for all luminescence measurements. This allowed inspection of a large area in a single view frame. Fluorescence microscopy was carried out with customized filter sets (Chroma Technology) for Cy3. To avoid photobleaching, the specimen was exposed to illumination only while taking images. Image Pro-plus version 6 with Scope Pro version 6 (Media Cybernetics, Inc.) was used for acquiring and analyzing images. We obtained fluorescence intensities for each sample by analyzing a 1.64 mm × 2.19 mm image section of each substrate. Background images were

obtained from an uncoated substrate and unmodified glass coverslips at the same conditions. Images from the experimental samples were corrected for uneven illumination with the help of these background images. Images of nanoparticle-coated glass coverslips were captured and compared with the image of a bare glass coverslip to test for the possibility of scattered light from metal particles. These images showed that the emission filters effectively removed the scattered light, so its contribution is negligible. The luminescence intensity of each sample was determined by measuring the mean intensity and subtracting the mean value of the background image.

III. Computational Methodology

The intensity of the luminophore at the proximity of metal nanoparticles can be written as[6,47]

$$I = C\eta(\omega_{flu})\sigma_{abs}(\omega_{abs})\left|K(\omega_{abs})\right|^2 I_{exc}(\omega_{abs})T \qquad (1)$$

Here, ω_{abs} is absorption frequency of the molecule, ω_{flu} is emission frequency of the molecule, $\eta(\omega_{flu})$ is quantum yield of emission, $\sigma_{abs}(\omega_{abs})$is absorption cross section of the molecule in vacuum, $I_{exc}(\omega_{abs})$ is exciting intensity in vacuum, C is a constant, T is integration time of the detector, and $K(\omega_{abs})$ is local field vector.

From the above expression, it can be seen that, by changing the local field for absorption $K(\omega_{abs})$ and/or quantum yield $\eta(\omega_{flu})$, we can change the intensity of luminescence. The absorption rate of the luminophore can be enhanced by increasing both the absorption coefficient of the luminophore itself and the local field intensity. On the other hand, the quantum yield of the luminophore can be influenced by varying the radiative and nonradiative decay rates.

Kümmerlen et al.[16] suggested that the quantum efficiency enhancement factor Y (ratio of quantum efficiencies in the presence of metal nanoparticles and without nanoparticles) can be calculated using the following equation:

$$Y = |L(\omega_{abs})|^2 Z(\omega_{flu}) \qquad (2)$$

The first term represents the enhancement of local electric field at the excitation frequency(ω_{abs}). The second term describes the change in quantum efficiency due to radiative and nonradiative decay rate enhancements at the emission frequency(ω_{flu}). The integrated near-field scattering cross section (Q_{nf}) at the excitation wavelength divided by the surface area of the spherical particle is a good measure of average $|L(\omega_{abs})|^2$.[48] The near-field scattering cross section can be calculated using the following equation[49]

$$Q_{nf} = 2\frac{r^2}{a^2}\sum_{n=1}^{\infty}\left\{\left|a_n\right|^2\left[(n+1)\left|h_{n-1}^{(1)}(ka)\right|^2 + n\left|h_{n+1}^{(1)}(ka)\right|^2\right] + (2n+1)\left|b_n\right|^2\left|h_n^{(1)}(ka)\right|^2\right\} \qquad (3)$$

where r is the distance from the center of the spherical nanoparticle and a is the radius of the nanoparticle. $k = (\varepsilon_m)^{1/2}\omega/c$, where ω is the optical frequency (radian per second), ε_m is the dielectric constant of the media, and c is the velocity of light in vacuum. The term $h_n^{(1)}$ is the spherical Henkel function of the first kind. a_n and b_n are well-known scattering coefficients.

The second factor in eq 2 is calculated using the corrected G-N model as suggested by Mertens et al.[1] Quantum efficiency is calculated as the ratio of radiative decay rate to total decay rate. Using the improved G-N model,[1,34] we calculated the modifications of the radiative decay rate (Γ_R) and total decay rate (Γ_{tot}) of luminophore in proximity to metal nanoparticles. This model is developed based on the assumption that the sizes of nanoparticles are much smaller than the wavelength. Thus, the retardation effect was accounted for by introducing a correction factor for radiative reaction and dynamic depolarization to modify the quasistatic polarizability of the nanoparticles. This model does not consider multipole radiation, and the interference between source dipole and induced dipole is neglected. In this model, the luminophore molecule is modeled as a classical dipole with dipole moment μ. For the radial dipole orientation, the expressions for Γ_R and Γ_{tot} for the luminophore molecule positioned at distance d from the surface of sphere with radius a and dielectric constant $\varepsilon = \varepsilon' + i\varepsilon''$ located in the medium of dielectric constant ε_m is as follows:[34]

$$\frac{\Gamma_{tot}^{\perp}}{\Gamma_R^{ref}} = 1 + \frac{3}{4(ka)^3}\sum_l l(l+1)\,\mathrm{Im}\left\{C_n\frac{\varepsilon-\varepsilon_m}{\varepsilon+\frac{l+1}{l}\varepsilon_m}\left(\frac{a}{a+d}\right)^{2l+4}\right\} \qquad (4)$$

$$\frac{\Gamma_R^{\perp}}{\Gamma_R^{ref}} = \left|1 + 2C_1\frac{\varepsilon-\varepsilon_m}{\varepsilon+2\varepsilon_m}\left(\frac{a}{a+d}\right)^3\right|^2 \qquad (5)$$

For the tangential dipole orientation, the expressions for Γ_R and Γ_{tot} are

$$\frac{\Gamma_{tot}^{//}}{\Gamma_R^{ref}} = 1 + \frac{3}{2(ka)^3}\sum_l (l+1)^2\,\mathrm{Im}\left\{C_l\frac{\varepsilon-\varepsilon_m}{\varepsilon+\frac{l+1}{l}\varepsilon_m}\left(\frac{a}{a+d}\right)^{2l+4}\right\} \qquad (6)$$

$$\frac{\Gamma_R^{//}}{\Gamma_R^{ref}} = \left|1 - C_1\frac{\varepsilon-\varepsilon_m}{\varepsilon+2\varepsilon_m}\left(\frac{a}{a+d}\right)^3\right|^2 \qquad (7)$$

In the above expressions, l is the angular mode number, and Γ_R^{ref} is the radiative decay rate of luminophore in the absence of nanoparticles. C_1 is the correction factor for radiation dumping and dynamic depolarization:

$$C_1 = \frac{1}{1 - \frac{ik^3\alpha}{6\pi} - \frac{k^2\alpha}{4\pi a}} \qquad (8)$$

α is the quasistatic polarizability,

$$\alpha = 4\pi a^3\frac{\varepsilon-\varepsilon_m}{\varepsilon+2\varepsilon_m} \qquad (9)$$

For $l \neq 1$, C_l is assumed to be 1.

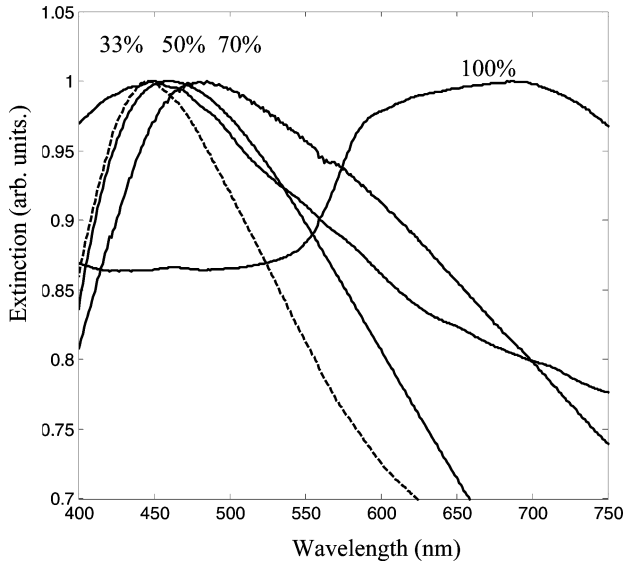

Figure 1. Normalized extinction spectra for Ag−Cu alloy nanoparticles at different percentages of copper. Solid lines show the extinction spectra of Ag−Cu nanoparticles in solution. Dotted line shows the extinction spectra of Ag−Cu nanoparticles with 33% Cu on APS coated glass slides.

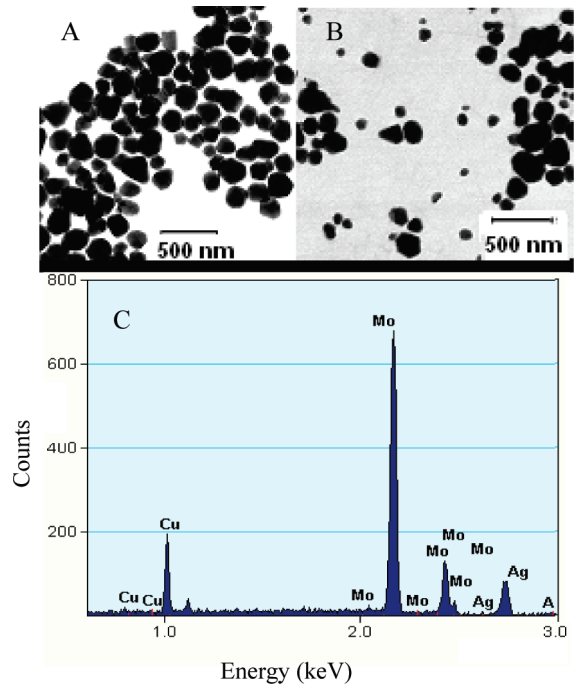

Figure 2. Transmission electron microscopy images of (A) 1:1 Ag−Cu nanoparticles and (B) 3:7 Ag−Cu nanoparticles. (C) STEM EDS spectra for 1:1 Ag−Cu alloy nanoparticles.

For better representation of experimental conditions, the source dipole orientation was averaged over all solid angles. This was achieved by averaging the results for decay rates obtained for radial and tangential orientations.

Dielectric constants for Ag−Cu nanoparticles of different compositions were calculated following the procedure described by Bruzzone.[50] The dielectric function was calculated using the semiempirical model based on Drude theory and experimental data. The experimental data used for this calculation were obtained by averaging the values for pure metals over the volume.[51] Drude contributions for nanostructure and bulk were calculated using the values of pure metal averaged over volumes. Though Ag−Cu cannot form a solid solution at room temperature as does Ag−Au, the surface plasmon resonance spectrum resembles that of alloy nanoparticles.[52] This is due to the fact that both silver and copper exist in the surface of Ag−Cu nanoparticles, and surface plasmon resonance is a surface phenomenon.[52]

IV. Result and Discussion

The UV−vis extinction spectra attributed to surface plasmon resonance of colloidal Ag−Cu nanoparticles show a single peak in the visible range. With increasing copper percentage, this SPR peak shifts to longer wavelengths (Figure 1). This result confirms that the nanoparticles are a bimetallic form of silver and copper and not a mixture of silver nanoparticles and copper nanoparticles.[53] The red-shifts of the SPR peaks with increasing copper concentration are attributed to the decrease in conductivity.[41] There is no visible difference between the position of extinction peaks of Ag−Cu nanoparticles in solution and on APS coated slides.

Transmission electron microscopy (Figure 2) of the colloidal Ag−Cu alloy nanoparticles indicated the particle size to be in the range of 130 to 200 nm (derived from a population of 100 particles). STEM EDS data (Figure 2C), confirms that the nanoparticles comprise both Ag and Cu. The concentration of nanoparticles increased with an increase in immersion time of APS coated glass slides in Ag−Cu colloidal solutions. As the copper percentage increased, the time required to attach the Ag−Cu colloids on glass slides also increased. For comparison, APS coated glass slides were allowed to soak in different composition Ag−Cu colloidal solutions until the concentrations of nanoparticles on glass slides were approximately the same. The sizes of different composition Ag−Cu nanoparticles coated on glass slides were also found to be approximately the same. The size of nanoparticles and particle density were measured using *Image J* software. From the SEM images of the Ag−Cu nanoparticles (Figure 3B,C), the average size of these nanoparticles on the glass slides was measured to be approximately 150 nm (derived from a population of 800 nanoparticles). SEM images of the Ag nanoparticles (Figure 3A) indicate their average size to be approximately 80 nm. AFM images of the Ag and Ag−Cu nanoparticles on glass slides are given in Figure 3D,E,F. The particle density for Ag nanoparticles was estimated to be 38 particles/μm^2. Particle density for Ag−Cu nanoparticles was estimated to be 20 particles/μm^2. It is difficult to obtain the same size and particle density for silver and silver−copper nanoparticles due to limitations of the synthesis techniques.

Luminescence intensity of Cy3 was observed to increase significantly in the vicinity of both Ag and Ag−Cu nanoparticles (Figure 4). The enhancement ratio for Ag and Ag−Cu nanoparticles was calculated by comparing luminescence intensity of the sample with the luminescence intensity of the luminophore coated on an APS coated glass substrate. In the case of copper nanoparticles, the enhancement ratio was calculated comparing the luminescence intensity with luminophore coated on PDDA coated glass slides. The Ag nanoparticles platform resulted in very strong enhancement (90.56 ± 19.45 times) for Cy3. As the quantum efficiency of dye Cy3 is very small, the enhancement effect is high. The Ag−Cu nanoparticles also showed enhancement (55.33 ± 15.23 times for 2:1 Ag−Cu, 30.00 ± 6.48 times for 1:1 Ag−Cu), but as the copper percentage in nanoparticles increased, the enhancement decreased. Finally, instead of enhancing, the Cu nanoparticles quenched (7.67 ± 5.01 times) the luminescence of Cy3. This may be because, in the vicinity of metal nanoparticles, both

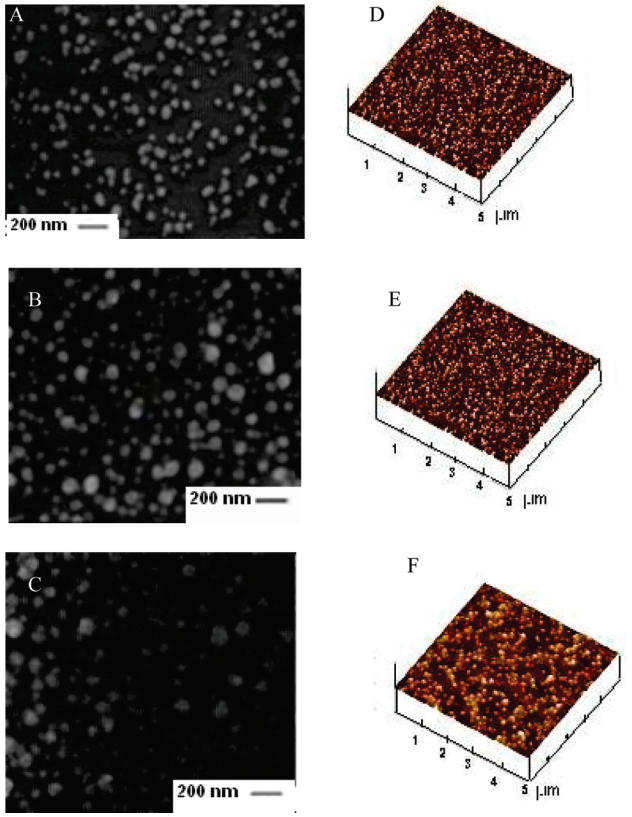

Figure 3. SEM images of (A) Ag nanoparticles (average size 78.81 ± 11.44 nm and particles density 38/μm^2), (B) 2:1 Ag−Cu nanoparticles (average size 157 ± 38 nm and particles density 19/μm^2), and (C) 1:1 Ag−Cu nanoparticles coated on glass substrates (average size 144 ± 12 nm and particles density 21/μm^2). AFM images of (D) Ag nanoparticles, (E) 2:1 Ag−Cu nanoparticles, and (F) 1:1 Ag−Cu nanoparticles coated on glass substrates.

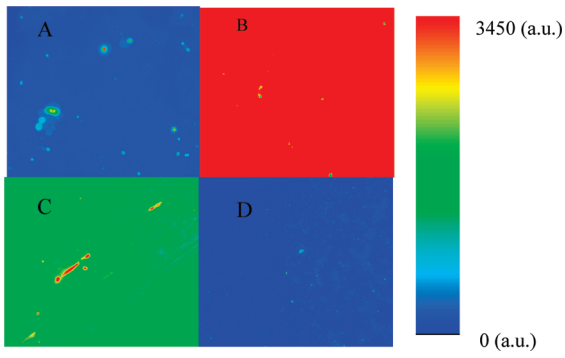

Figure 4. Pseudo-colored image (intensity scale increases from blue to red) of Cy3 coated on (A) glass, (B) Ag nanoparticles, (C) 1:1 Ag−Cu nanoparticles, and (D) Cu nanoparticles.

the radiative decay rate and the nonradiative decay rates increase, and as percentage of Cu increases, the nonradiative decay rate also increases, eventually surpassing the radiative decay rate.

We calculated the modified overall quantum efficiency at the proximity of different compositions of Ag−Cu nanoparticles based on the model suggested by Kümmerlen et al.,[16] which includes both excitation and emission enhancement factors as discussed in section III. The absorption enhancement factor was calculated based on the enhancement of local electric field at the excitation frequency (ω_{abs}). The corrected G-N model[1,34] model was used to calculate the quantum efficiency change due to radiative and the nonradiative decay rate enhancements. Calculations were done to corroborate experimental results and

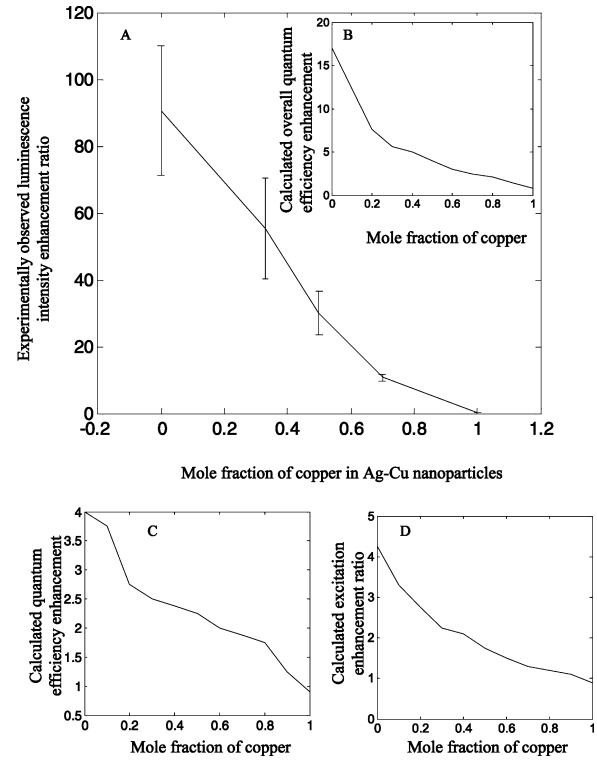

Figure 5. (A) Experimentally observed luminescence enhancement ratio of Cy3 in the proximity of different compositions of Ag−Cu nanoparticles. (B) Inset shows theoretically calculated overall luminescence quantum efficiency enhancement ratio. (C) Calculated quantum efficiency enhancement factor due to emission enhancement. (D) Calculated excitation rate enhancement factor as a function of composition of Ag−Cu nanoparticles.

to establish the optimum size of nanoparticles. Figure 5A,B shows the theoretically calculated modified overall quantum efficiency and the experimentally observed luminescence enhancement ratio of luminophore Cy3 in the vicinity of different compositions of Ag−Cu nanoparticles. The calculations were done assuming the size of nanoparticles to be 150 nm and the separation distance between nanoparticles and luminophore molecules to be 13 nm to compare with experimental results. The surrounding dielectric medium was assumed to be poly(vinyl alcohol). The enhancement of local electric field amplitude ($|L_{abs}^2|$) was calculated at the absorption frequency of Cy3 (550 nm). The quantum efficiency change ($Z(\omega_{flu})$) due to radiative and nonradiative decay rate enhancement was calculated at 570 nm emission wavelength, which is the emission peak for Cy3. The quantum efficiency was calculated taking into account all multipole modes up to $l = 100$. Dipole orientation was assumed to be averaged over all solid angles. It can be seen from Figure 5A and B that both theoretical and experimental results show the same trend in which an increase in copper percentage in nanoparticles decreases the enhancement effect, with pure copper quenching luminescence. The theoretically calculated emission enhancement factor and the excitation enhancement factor are separately shown in Figure 5C,D, respectively. We can see that both emission and excitation have comparable effects on overall quantum efficiency change. Some reasons for the discrepancy in numerical values between theoretical and experimental results are the differences in experimental geometry (nanoparticles are not in a homogeneous dielectric environment, all the nanoparticles were not of spherical shape and not of same size, luminophore nanostructures separation distance is not precise) with respect to theoreti-

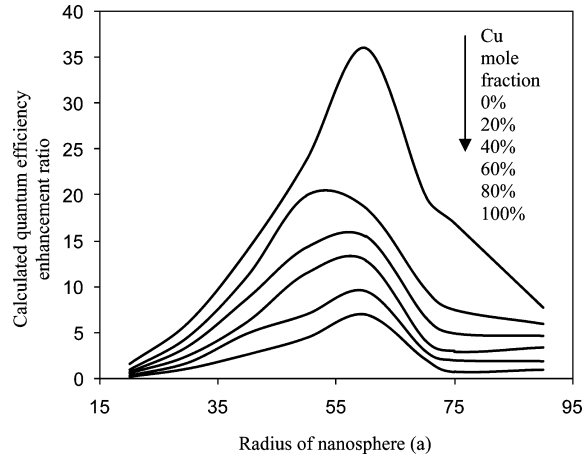

Figure 6. Quantum efficiency enhancement ratio of Cy3 in the proximity of different diameter Ag−Cu nanoparticles at different compositions embedded in a dielectric medium of poly(vinyl alcohol). Luminophore-nanoparticles separation distance is assumed to be 13 nm.

cal calculations, which assumed uniformity in these parameters. It can also be because we observed the luminescence intensity of the image over the entire bandwidth of filters used for fluorescence microscopy, not at any particular wavelength.

It is known that quantum efficiency enhancement depends on the size of spherical nanoparticles.[1] Figure 6 shows the dependencies of quantum efficiency enhancement on the size of Ag−Cu nanoparticles at the fluorophore−nanoparticle separation distance of 13 nm. The calculation for Figure 6 was done considering the same emitter−particle orientation and surrounding conditions as for Figure 5. It can be seen from Figure 6 that there is an optimum size of nanoparticles for which quantum efficiency enhancement is maximum. The coupling between the emission of the luminophore and the plasmon mode increases as the size of the nanoparticles decreases, and coupling efficiency of emission at far field through nanoparticle scattering increases as the size of nanoparticles increases. Both of these coupling phenomena are responsible for enhancement of quantum efficiency. Spectral overlap between the absorption and emission spectra of luminophore and surface plasmon resonance spectra of metal nanoparticles is very important for optimum luminescence enhancement.[14,35,54] Some theoretical and experimental studies have suggested that luminescence enhancement is largest when the emission wavelength is slightly red-shifted from that of the plasmon resonance.[35,47,55] When the size of the particle increases, the plasmon resonance is shifted to longer wavelength and broadened and decreases in magnitude due to dynamic polarization.[56] So, there exists an optimum diameter. We can see from Figure 6 that the optimum radius for Ag, Ag−Cu, and also Cu nanoparticles is approximately 60 nm. At this optimum diameter, even Cu nanoparticles show enhancement instead of quenching. So, it can be inferred that, if we can synthesize alloy nanoparticles of optimum diameter using advanced methods like electron beam lithography, we can elucidate the effect of composition on metal-enhanced luminescence better.

V. Conclusions

In summary, in this work metal-enhanced luminescence/quenching of luminophore Cy3 is explored in the vicinity of Ag−Cu alloy nanoparticles at different compositions. The effect of composition of Ag−Cu alloy nanoparticles on luminescence enhancement is studied. We have shown that strongest enhancement is observed on the Ag nanoparticle platform, and as the percentage of copper increases in the nanoparticles, the enhancement decreases. At pure copper nanoparticle platforms, the luminescence is quenched. A simple technique to tune the brightness of a luminophore by changing the composition of alloy nanoparticles is presented. Experimentally obtained data for luminescence change qualitatively match with theoretical calculations. We believe such manipulation in luminescence brightness of a dye will introduce different applications for luminescence emission. We expect the quenching effect of copper nanoparticles to encourage the utilization of these nanoparticles as an inexpensive alternative to gold in biological applications such as homogeneous and competitive fluorescence immunoassay, detection of DNA hybridization, competitive hybridization assay, and also optoelectronics.

Acknowledgment. This material is based upon work supported by the National Science Foundation under grant no CMS-409401.

References and Notes

(1) Mertens, H.; Koenderink, A. F.; Polman, A. *Phys. Rev. B* **2007**, *76*, 115123.
(2) Aslan, K.; Holley, P.; Geddes, C. D. *J. Immunol. Methods* **2006**, *312*, 137.
(3) Lakowicz, J. R. *Anal. Biochem.* **2001**, *298*, 1.
(4) Lakowicz, J. R.; Malicka, J.; Gryczynski, I.; Gryczynski, Z.; Geddes, C. D. *J. Phys. D: Appl. Phys.* **2003**, *36*, R240–R249.
(5) Lakowicz, J. R.; Shen, Y.; D'Auria, S.; Malicka, J.; Fang, J.; Gryczynski, Z.; Gryczynski, I. *Anal. Biochem.* **2002**, *301*, 261.
(6) Azoulay, J.; Débarre, A.; Richard, A.; Tchénio, P. *Europhys. Lett.* **2000**, *51*, 374.
(7) Campion, A.; Gallo, A. R.; Harris, C. B.; Robota, H. J.; Whitmore, P. M. *Chem. Phys. Lett.* **1980**, *73*, 447.
(8) Mertens, H. Controlling plasmon-enhanced luminescence, Utrecht University, 2007.
(9) Schneider, G.; Decher, G.; Nerambourg, N.; Praho, R.; Werts, M. H. V.; Blanchard-Desce, M. *Nano Lett.* **2006**, *6*, 530.
(10) Ray, K.; Badugu, R.; Lakowicz, J. R. *Langmuir* **2006**, *22*, 8374.
(11) Pan, S.; Rothberg, L. J. *J. Am. Chem. Soc.* **2005**, *127*, 6087.
(12) Cheng, D.; Xu, Q.-H. *Chem. Commun.* **2007**, 248.
(13) Zhang, J.; Matveeva, E.; Gryczynski, I.; Leonenko, Z.; Lakowicz, J. R. *J. Phys. Chem. B* **2005**, *109*, 7969.
(14) Tam, F.; Goodrich, G. P.; Johnson, B. R.; Halas, N. J. *Nano Lett.* **2007**, *7*, 496.
(15) Malicka, J.; Gryczynski, I.; Gryczynski, Z.; Lakowicz, J. R. *Anal. Biochem.* **2003**, *315*, 57.
(16) Kümmerlen, J.; Leitner, A.; A; Brunner, H.; A; Aussenegg, F. R.; Wokaun, A *Mol. Phys.* **1993**, *80*, 1031.
(17) Aslan, K.; Lakowicz, J. R.; Geddes, C. D. *Anal. Bioanal. Chem.* **2005**, *382*, 926.
(18) Pompa, P. P.; Martiradonna, L.; Torre, A. D.; Sala, F. D.; Manna, L.; Vittorio, M. D.; Calabi, F.; Cingolani, R.; Rinaldi, R. *Nat. Nanotechnol.* **2006**, 1.
(19) Dulkeith, E.; Ringler, M.; Klar, T. A.; Feldmann, J.; MunozJavier, A.; Parak, W. J. *Nano Lett.* **2005**, *5*, 585.
(20) Aslan, K.; Malyn, S. N.; Geddes, C. D. *J. Fluoresc.* **2007**, *17*, 7.
(21) Aslan, K.; Malyn, S. N.; Geddes, C. D. *Chem. Phys. Lett.* **2008**, *453*, 222.
(22) Ray, K.; Chowdhury, M. H.; Lakowicz, J. R. *Anal. Chem.* **2007**, *79*, 6480.
(23) Zhang, Y.; Aslan, K.; Previte, M. J. R.; Geddes, C. D. *Appl. Phys. Lett.* **2007**, *90*, 173116.
(24) Dorfman, A.; Kumar, N.; Hahm, J.-i. *Langmuir* **2006**, *22*, 4890.
(25) Dorfman, A.; Kumar, N.; Hahm, J.-i. *Adv. Mater.* **2006**, *18*, 2685.
(26) Kumar, N.; Dorfman, A.; Hahm, J.-i. *Nanotechnology* **2006**, *17*, 2875–2881.
(27) Kato, N.; Caruso, F. *J. Phys. Chem. B* **2005**, *109*, 19604.
(28) Ao, L.; Gao, F.; Pan, B.; He, R.; Cui, D. *Anal. Chem.* **2006**, *78*, 1104.
(29) Zai-Sheng, W.; Jian-Hui, J.; FU, L.; Guo-Li, S.; Ru-Qin, Y. *Anal. Biochem.* **2006**, *353*, 22.
(30) Dubertret, B.; Calame, M.; Libchaber, A. J. *Nat. Biotechnol.* **2001**, *19*, 365.
(31) Imahori, H.; Fukuzumi, S. *Adv. Mater.* **2001**, *13*, 1197.
(32) Ruppin, R. *J. Chem. Phys.* **1982**, *76*, 1681.
(33) Gersten, J.; Nitzan, A. *J. Chem. Phys.* **1981**, *75*, 1139.

(34) Mertens, H.; Polman, A. Strong luminescence quantum efficiency enhancement near prolate metal nanoparticles: dipolar versus higher-order modes. In *ArXiv e-prints*, **2007**; Vol *711*.
(35) Chen, Y.; Munechika, K.; Ginger, D. S. *Nano Lett.* **2007**, *7*, 690.
(36) Weimer, W. A.; Dyer, M. J. *Appl. Phys. Lett.* **2001**, *79*, 3164.
(37) Jensen, T. R.; Schatz, G. C.; Duyne, R. P. V. *J. Phys. Chem. B* **1999**, *103*, 2394.
(38) Li, Z. Y.; Wilcoxon, J. P.; Yin, F.; Chen, Y.; Palmer, R. E.; Johnston, R. L. *Faraday Discuss.* **2008**, *138*, 363.
(39) Zhang, J.; Liu, H.; Wang, Z.; Ming, N. *J. Solid State Chem.* **2007**, *180*, 1291.
(40) Song, J.; Li, H.; Li, J.; Wang, S.; Zhou, S. *Appl. Opt.* **2002**, *41*, 5413.
(41) Hirai, M.; Kumar, A. *J. Appl. Phys.* **2006**, *100*, 0143091.
(42) Hirai, M.; Kumar, A. *J. Electron. Mater.* **2007**, *36*, 1574.
(43) Chandran, R. S.; John, S. E.; Amit, M. *J. Chem. Phys.* **2005**, *122*, 061103.
(44) Hongjin, J.; Kyoung-sik, M.; Wong, C. P. Synthesis of Ag-Cu alloy nanoparticles for lead-free interconnect materials; Advanced Packaging Materials: Processes, Properties and Interfaces, 2005. Proceedings. International Symposium on, 2005.
(45) Aslan, K.; Lakowicz, J. R.; Geddes, C. D. *J. Phys. Chem. B* **2005**, *109*, 6247.
(46) Male, K. B.; Hrapovic, S.; Liu, Y.; Wang, D.; Luonga, J. H. T. *Anal. Chim. Acta* **2004**, *516*, 35–41.
(47) Thomas, M.; Greffet, J.-J.; Carminati, R. *Appl. Phys. Lett.* **2004**, *85*, 3863.
(48) Nakamura, T.; Hayashi, S. *Jpn. J. Appl. Phys.* **2005**, *44*, 6833–6837.
(49) Messinger, B. J.; Raben, K. U. v.; Chang, R. K.; Barber, P. W. *Phys. Rev. B* **1981**, *24*, 649.
(50) Bruzzone, S.; Malvaldi, M.; Arrighini, G. P.; Guidotti, C. *J. Phys. Chem. B* **2006**, *110*, 11050.
(51) Palik, E. D. *Handbook of Optical Constants of Solids*, 1st ed.; Academic Press Inc.: Orlando, 1985.
(52) Itakura, T.; Torigoe, K.; Esumi, K. *Langmuir* **1995**, *11*, 4129.
(53) Zhang, J.; Liu, H.; Wang, Z.; Ming, N. *J. Solid State Chem.* **2007**, *180*, 1291.
(54) Yeechi, C.; Keiko, M.; Ilan Jen-La, P.; Andrea, M. M.; Sara, E. S.; Younan, X.; David, S. G. *Appl. Phys. Lett.* **2008**, *93*, 053106.
(55) Bharadwaj, P.; Novotny, L. *Opt. Express* **2007**, *15*, 14266.
(56) Meier, M.; Wokaun, A. *Opt. Lett.* **1983**, *8*.

JP900294Z